

# CHEMISTRY

## A European Journal

A Journal of



### Accepted Article

**Title:** Topotactic conversion of alkali-treated intergrowth germanosilicate CIT-13 into single crystalline ECNU-21 zeolite as shape-selective catalyst for ethylene oxide hydration

**Authors:** Xue Liu, Wenting Mao, Jingang Jiang, Xinqing Lu, Mingming Peng, Hao Xu, Lu Han, Shun-ai Che, and Peng Wu

This manuscript has been accepted after peer review and appears as an Accepted Article online prior to editing, proofing, and formal publication of the final Version of Record (VoR). This work is currently citable by using the Digital Object Identifier (DOI) given below. The VoR will be published online in Early View as soon as possible and may be different to this Accepted Article as a result of editing. Readers should obtain the VoR from the journal website shown below when it is published to ensure accuracy of information. The authors are responsible for the content of this Accepted Article.

**To be cited as:** *Chem. Eur. J.* 10.1002/chem.201900173

**Link to VoR:** <http://dx.doi.org/10.1002/chem.201900173>

Supported by  
**ACES**

WILEY-VCH

## FULL PAPER

# Topotactic conversion of alkali-treated intergrown germanosilicate CIT-13 into single-crystalline ECNU-21 zeolite as shape-selective catalyst for ethylene oxide hydration

Xue Liu,<sup>[a]</sup> Wenting Mao,<sup>[b]</sup> Jingang Jiang,<sup>[a]</sup> Xinqing Lu,<sup>[a]</sup> Mingming Peng,<sup>[a]</sup> Hao Xu,<sup>\*,[a]</sup> Lu Han,<sup>\*,[b,c]</sup> Shun-ai Che,<sup>[b,c]</sup> and Peng Wu<sup>\*,[a]</sup>

**Abstract:** Conversion of alkali-treated intergrowth germanosilicate CIT-13 into single crystalline high-silica ECNU-21 (named after *East China Normal University*) zeolite, with a novel topology and a highly crystalline zeolite framework, has been realized via a creative top-down strategy involving mild alkaline treatment-induced multistep process of structural degradation and reconstruction. Instead of acid treatment, the hydrolysis in ammonia aqueous solution not only disconnected readily the chemically weak Ge(Si)-O-Ge bonds located within interlayer double four ring (D4R) units of CIT-13 but also cleaved the metastable Si-O-Si bonds therein. This leads to an extensive removal of D4R units, and also generates the silanol groups on adjacent silica-rich layers which are then condensed into a novel daughter structure upon calcination. Individual oxygen bridges in reassembled ECNU-21 replace the Ge-rich D4R units in CIT-13, which eliminates the original intergrowth phenomenon along *b*-axis. With ordered crystalline structure of 10-ring (R) channels as well as suitable Ge-related acid sites, ECNU-21 serves as a stable solid-acid catalyst for the shape-selective hydration of ethylene oxide (EO) to ethylene glycol (EG) at greatly reduced H<sub>2</sub>O/EO ratios and reaction temperature in comparison to non-catalytic industrial process.

## Introduction

Zeolites with well-defined crystalline structures and unique microporosities of molecular sizes are employed widely as useful adsorbents, ion-exchangers and in particular heterogeneous catalysts in petrochemical industry.<sup>[1]</sup> To date, 239 known topologies have been recognized by International Zeolite Association (IZA), including nine partially disordered materials that consist of variable structures (usually known as intergrowth

zeolites).<sup>[2]</sup> Beta zeolite (\*BEA) is one of the most studied intergrowth zeolites, the framework of which contains intergrown stackings of two similar polymorphs A and B with a ratio of 44 : 56.<sup>[3]</sup> Having the same building layers, other polymorphs C, C<sub>H</sub>, D, and E have also been proposed or experimentally verified for the Beta family.<sup>[3b,3c,4]</sup> A more complex zeolite ITQ-39 containing three polymorphs was reported as an effective catalyst for the alkylation of aromatics.<sup>[5]</sup> ECNU-5 zeolite built from the polytype stackings of MWW layers highly resembles SSZ-70 zeolite (\*SVY).<sup>[6]</sup> In the field of intergrowth zeolites, the efforts mainly focus on resolving the crystal structure,<sup>[7]</sup> exploring the unique catalytic performance<sup>[6a]</sup> and synthesizing the pure polymorph.<sup>[7]</sup> The latter is of high importance in terms of crystallographic interests and catalytic applications. As a typical representative, the germanate (FOS-5)<sup>[8]</sup> and germanosilicate (ITQ-17)<sup>[9]</sup> with a pure polymorph C (BEC) structure in Beta family have been hydrothermally synthesized via incorporating germanium into the framework to stabilize the D4R units. Besides, the successful synthesis of CIT-1 (CON topology) is also another example, which is considered to be the pure polymorph B of the SSZ-26 and SSZ-33 family (both SSZ-26 and SSZ-33 are intergrowth of polymorph A and B).<sup>[10]</sup> Later, the pure polymorph C of this zeolite family was also reported, known as ITQ-24 zeolite.<sup>[11]</sup>

Recently, a novel intergrowth Ge-zeolite CIT-13 (\*CTH topology) has been reported, consisting of the *cfi*-layers interconnected by D4R units and intersected 14- and 10-R channels.<sup>[12]</sup> Subsequently, two germanosilicates of NUD-2<sup>[13]</sup> and SAZ-1<sup>[14]</sup> were announced to possess the structures analogous to CIT-13. The 14-R channels running parallel to the crystallographic *c*-axis bear a striking resemblance to the UTL topology, while the arrangement of 10-R channels along *b*-axis is ill-defined, giving rise to two or more possible framework structures (AAAA sequence and ABAB sequence and more), which was revealed by the serious mosaicity along *b*-axis in the TEM images.<sup>[12b]</sup> In other words, the random or irregular location of D4R subunits along *c* direction induced the stacking faults.

In the past years, germanosilicates have set off research upsurge due to modifiable structure prosperity benefiting from the relatively weak Ge(Si)-O-Ge bonds in D4R units, since they are potential precursors useful for postsynthesizing a variety of novel zeolite structures hardly generated by direct hydrothermal synthesis. The typical assembly-disassembly-organization-reassembly (ADOR) strategy<sup>[15]</sup> has been proved to be highly effective in selective removing interlayer Ge-rich D4R units in acidic media and converting 3-dimensional (3D) germanosilicates to 2D layered intermediates, followed by reconstruction to several daughter structures with the assistant of ammonia or silane agent. Though the ADOR strategy has achieved success in the structural reconstruction of UTL,<sup>[15]</sup> IWW,<sup>[16]</sup> ITH,<sup>[17]</sup> ITR,<sup>[17]</sup> IWR,<sup>[17]</sup> SAZ-1<sup>[14]</sup>

[a] X. Liu, Dr. J. Jiang, Dr. H. Xu, M. Peng, Dr. X. Lu, Prof. P. Wu  
Shanghai Key Laboratory of Green Chemistry and Chemical Processes  
School of Chemistry and Molecular Engineering, East China Normal University  
North Zhongshan Road 3663, Shanghai, 200062 (P.R. China)  
E-mail: pwu@chem.ecnu.edu.cn, hxu@chem.ecnu.edu.cn

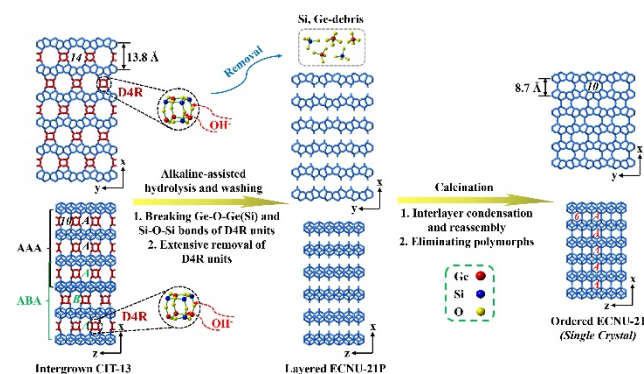
[b] W. Mao, Prof. L. Han, Prof. S. Che  
State Key Laboratory of Metal Matrix Composites  
School of Chemistry and Chemical Engineering, Shanghai Jiao Tong University  
Dongchuan Road 800, Shanghai, 200240, (P.R. China)

[c] Prof. L. Han, Prof. S. Che  
School of Chemical Science and Engineering, Tongji University  
Siping Road 1239, Shanghai, 200092, (P.R. China)

Supporting information for this article is given via a link at the end of the document.

## FULL PAPER

and UOV<sup>[18]</sup> germanosilicates, only three highly ordered materials with the code of OKO, PCR and PCS derived from UTL have been recognized by IZA. Our group also proposed an acid treatment strategy to obtain structure derivatives from UTL zeolite via simply controlling the treatment time.<sup>[19]</sup> Since the intergrowth of CIT-13 originates from the random or irregular location of D4R subunits on the (010) plane, we anticipate the disordered phenomenon are possibly eliminated after fully removing the interlayer D4R units, forming a layered intermediate and thereafter reconstructing a novel single crystalline structure. Although the original extra-large pore system would be sacrificed, the newly constructed daughter structure could be useful for shape-selective catalysis. For the purpose of ADOR top-down synthesis, the key step is the formation of the layered precursor. However, a sufficiently large amount of Ge atoms are not always enough to unlock the interlayer linkage completely via acid treatment.<sup>[20]</sup> And the metastable Si-O-Si interlayer bonds vertical to the layers in D4R units are supposed to prohibit the full separation of the layers, making the framework hardly degradable and changeable against acid hydrolysis. Unfortunately, Ge-CIT-13 encountered failure to form a lamellar product in acidic media. The more detailed discussion of the reasons will be provided (*vide post*).



**Scheme 1.** Structural conversion processes from intergrown CIT-13 into ordered ECNU-21 via alkali-induced strategy. Mild alkaline media dislodges D4R units in polymorph CIT-13 completely and further reassembly to single crystalline high-silica zeolite ECNU-21 upon calcination.

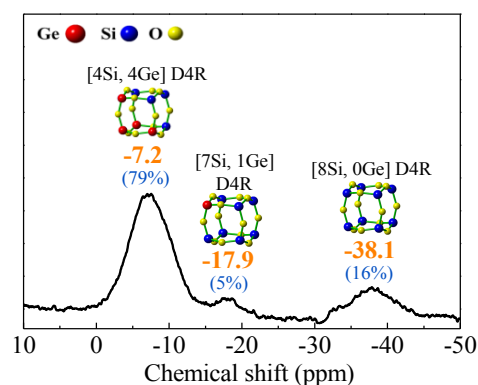
Herein, we report the systematic removal of the randomly arranged D4R units in \*CTH through a creative top-down strategy in basic media of ammonia aqueous solution, eliminating the intergrowth structures of CIT-13 and transferring it into a novel single-crystalline structure ECNU-21. This process can also be recognized as an inverse sigma transformation.<sup>[21]</sup> Scheme 1 depicts the structural degradation and reconstruction processes for the synthesis of fully ordered ECNU-21 zeolite with intergrowth CIT-13 as a starting material, involving (i) chemoselective dislodgement of Si-O-Si bond-containing D4R units in CIT-13 via alkaline-assisted hydrolysis, thereby resulting in high-silica precursor ECNU-21P consisting of crystalline monolayers; (ii) spontaneous condensation of the neighboring *cfi*-layers upon calcination to reconstruct the daughter structure ECNU-21 with 1D 10-R channels. The key to achieve highly ordered ECNU-21

zeolite is employing mild alkaline media to cleave not only chemically weak Ge(Si)-O-Ge bonds but more importantly the metastable Si-O-Si bonds vertical to the layers in D4R subunits, inducing disassembly and reconstruction of germanosilicate frameworks. With moderate Ge-derived Lewis acidity confined in 10-R channels, the ordered ECNU-21 exhibited a promising shape-selective catalyst in the ethylene oxide hydration reaction. This is also the first study to ever report the catalytic performance of germanosilicates serving as solid Lewis acid catalyst in the hydration reactions.

## Results and Discussion

### Characterization of high-silica zeolite ECNU-21

We firstly attempted to remove the D4R subunits from \*CTH topology by performing the typical acid-assisted ADOR procedure on the calcined Ge-rich CIT-13 (Si/Ge = 3.7) that was hydrothermally synthesized using 1,2-dimethyl-3-(3-methylbenzyl) imidazolium hydroxide as organic structure-directing agent (OSDA) (Figure S1-S3). Irrespective of using either HCl aqueous solution with varied concentrations (0.1 - 4.0 M) (Figure S4) or identical HNO<sub>3</sub> solution via altering the treatment time (Figure S5), the calcined Ge-rich CIT-13 experienced only limited structural collapse and then rapidly reconstructed to stable structure analogous to the \*CTH topology. The unique structural property of CIT-13 upon acid treatments is probably related to the framework composition and the Ge location in D4R units.<sup>[20]</sup>

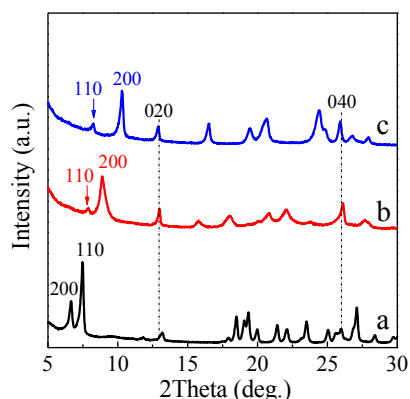


**Figure 1.** <sup>19</sup>F MAS NMR spectrum of the as-synthesized CIT-13 sample. The numbers in parentheses show the percentages of three major D4R units with different Si/Ge ratios.

As an efficient means of characterization, solid-state <sup>19</sup>F MAS NMR spectroscopy has been employed to probe the location and distribution of Ge atoms in the framework, because F<sup>-</sup> ions prefer to locate in the center of D4R units and their chemical environments varied with the configurations of surrounding Si and Ge.<sup>[20]</sup> As-synthesized CIT-13 displayed a major peak at -7.2 ppm along with two other resonances at -17.9 and -38.1 ppm (Figure 1), assigned to F<sup>-</sup> ions located in the D4R units with the

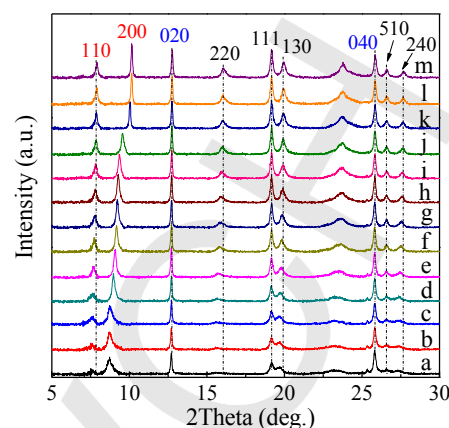
## FULL PAPER

compositions of [4Si, 4Ge], [7Si, 1Ge] and [8Si, 0Ge], respectively.<sup>[20]</sup> The relatively stable Si-O-Si bonds vertical to the layers occupy at least 21% of D4R units arising from the [7Si, 1Ge] and [8Si, 0Ge] groups in CIT-13, not to mention those from the [4Si, 4Ge] group. Thus, Ge-CIT-13 zeolite was failed to evolve to new crystalline structures. Moreover, Si-O-Si bonds are known to be stable in acid solution but unstable in alkaline media. It would be a rational way to remove extensively the D4R units from CIT-13 by carrying out the ADOR procedures in alkaline media like ammonia aqueous solution.



**Figure 2.** PXRD patterns of calcined CIT-13 (a), ammonia aqueous solution treatment-derived layered precursor ECNU-21P (b) and subsequently calcined sample ECNU-21 (c).

Subsequently, the layered intermediate ECNU-21P was achieved readily via stirring a suspension of calcined Ge-CIT-13 and  $\text{NH}_3\cdot\text{H}_2\text{O}$  aqueous solution. As demonstrated by the PXRD pattern of ECNU-21P remarkably distinct from original CIT-13 (Figure 2), the layer-related 200 reflection shifted to a higher  $2\theta$  angle of  $8.9^\circ$  (ca.  $6.4^\circ$  for pristine CIT-13), indicating the significant narrowing of the interlayer  $d$ -spacing. Meanwhile, the 110 reflection also became weaker and moved to higher angle of  $2\theta \approx 8.2^\circ$ . Note that there was a considerable intensity loss of numerous peaks in the  $2\theta$  range of  $17^\circ - 30^\circ$ , implying the decline of crystallinity as a result of the distinctive structural disassembly. In contrast, the intralayer structure-related  $0k0$  reflections including 020 and 040 were well-preserved, implying that the long-range structure order within Si-rich layers was well-maintained during hydrolysis process. Upon subsequent calcination at 823 K for 6 h, the precursor ECNU-21P underwent a structural reconstruction, evolving from 2D structure to a new 3D ECNU-21 with a high-silica framework ( $\text{Si}/\text{Ge} = 33$ ) and a comparable crystallinity to the original CIT-13. The well-resolved 200 reflection also became sharper with a further right-shift to  $2\theta = 10.3^\circ$  (Figure 2c). ECNU-21 could be analogous to IPC-15 zeolite,<sup>[14]</sup> according to the description in the literature. Nevertheless, the ECNU-21 zeolite derived from Ge-zeolite CIT-13 via alkali treatment possessed higher crystallinity and more ordered structure than IPC-15 post-synthesized from the germanosilicate SAZ-1 through acid-assisted ADOR route. Moreover, it is worth pointing out that ECNU-21 and IPC-15 are distinctive in PXRD patterns (Figure S6), indicative of the differences in both structure and purity.



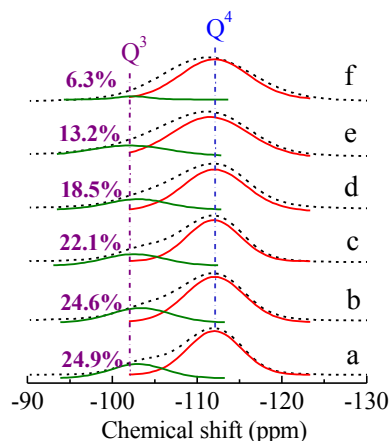
**Figure 3.** *In-situ* PXRD patterns revealing a gradual evolution from two-dimensional layered structure of ECNU-21P to three-dimensional crystalline zeolite of ECNU-21 depending on continuous heating at 298 K (a), 323 K (b), 373 K (c), 423 K (d), 473 K (e), 523 K (f), 573 K (g), 623 K (h), 673 K (i), 723 K (j), 773 K (k), 823 K (l) and 873 K (m) with a heating rate of 30 K min<sup>-1</sup> (from bottom to top).

The reassembly process from 2D ECNU-21P precursor to 3D ECNU-21 upon calcination was precisely traced via the *in-situ* PXRD measurement (Figure 3). Along with the continuous heating from 298 K to 823 K, the 200 reflection increased in intensity, accompanied by gradual shift of  $2\theta$  position from  $8.9^\circ$  to  $10.3^\circ$ , because of the condensation of neighboring *cff*-layers and the decline of the average interlayer  $d$ -spacing (Figure S7). The drastic structural change upon calcination occurred in the temperature ranges of 423 - 573 K and 673 - 823 K, as revealed by the variation trend of the  $d$ -spacing of layer-related 200 reflection. The *in-situ* PXRD measurement also showed a steady enhancement of the intensity of 110 and 220 reflections, reaching the maximum value at 823 K. The reassembly process was supposed to finish at 823 K, after which point the interlayer distance levelled off (Figure S7). Simultaneously, the slight intensity enhancement was also observed for the 020, 111, 130, 040, 510 and 240 reflections due to the recovery of a long-range ordered structure. Besides, the  $2\theta$  positions of intralayer-related 020 and 040 reflections almost stayed unchanged independent of the temperature-induced condensation process, implying the Si-rich CIT-13 sheets almost kept intact upon calcination. The reassembled ECNU-21 structure was well preserved and thermally stable against a further calcination at 873 K. In spite of the dramatic structural change in the ammonium solution treatment and subsequent calcination process, the ECNU-21 crystals still preserved the thin platelet morphology similar to the pristine CIT-13 (Figure S8).

*Ex-situ*  $^{29}\text{Si}$  MAS NMR spectra were employed to obtain more information for the structural change in the respect of silicon coordination during the structural degradation and reconstruction processes. To confirm the accurate position of  $(\text{SiO})_3\text{Si}(\text{OH})$  groups ( $\text{Q}^3$ ) in the spectra,  $^1\text{H}$ - $^{29}\text{Si}$  cross-polarization MAS NMR spectrum of ECNU-21 was firstly performed (Figure S9) and the resonance band at about -101.8 ppm was ascribed to  $\text{Q}^3$  groups. The pristine Ge-rich CIT-13 zeolite showed a resonance signal at

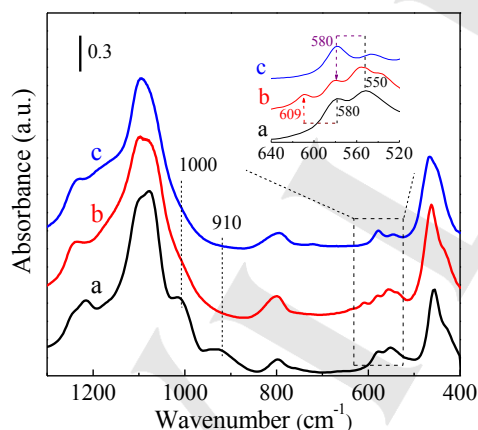


## FULL PAPER



**Figure 4.** Ex-situ  $^{29}\text{Si}$  MAS NMR spectra (dotted lines) and fitting results (solid lines) of as-made ECNU-21P samples (a), and after calcination at 423 K (b), 523 K (c), 623 K (d), 723 K (e) and 823 K (f) for 6 h, respectively.

$\delta = -101.9$  ppm, which is assigned to the  $\text{Q}^3$  and  $1\text{Si}3\text{Ge}$  groups,<sup>[22]</sup> accounting for 8.1% population (Figure S10 and Table S2). The hydrolysis in ammonia aqueous solution led to a rapid increase of  $\text{Q}^3$  groups to 24.9% (Figure 4), as a result of an extensive removal of Ge-containing D4R units located between the *cfi*-layers. At the initial heating stage ( $T < 523$  K) of reassembly process, a slight decrease of  $\text{Q}^3$  groups together with a minor increase of signals in the range of -112 to -114 ppm arising from  $\text{Si}(\text{OSi})_4$  ( $\text{Q}^4$ ) groups was observed, indicative of the condensation of adjacent layers. In the higher temperature region, the population of  $\text{Q}^3$  species was sharply decreased to a minimum value of 6.3% at 823 K, meaning that defects still existed in the final ECNU-21 zeolite. At this temperature, the *d*-spacing of layer-related 200 reflection ( $d_{200}$ ) reached a minimum value of ca. 8.7 Å



**Figure 5.** IR spectra in the framework vibration region of CIT-13 (a), CIT-13S (b) and ECNU-21 (c) after calcination. The inset shows the enlarged region of 640 - 520  $\text{cm}^{-1}$ .

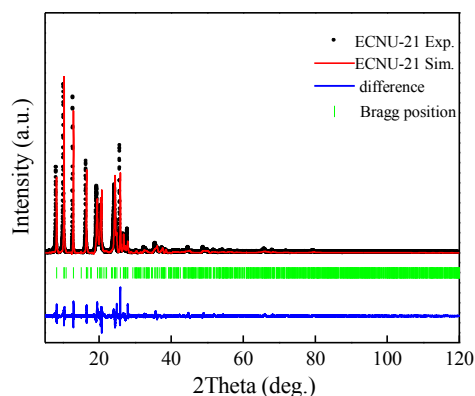
at 823 K. Moreover, the extensive removal of Ge-rich D4R subunits made the resonances from -102 to -110 ppm disappear (Figure S7). Both PXRD and  $^{29}\text{Si}$  MAS NMR investigations suggested a full condensation of adjacent layers was completed

for the resultant ECNU-21 zeolite, which are attributed to Ge-containing groups  $n\text{Si}(4-n)\text{Ge}$ .<sup>[23]</sup>

The IR technique is also a sensitive method for characterizing structural change. As displayed in Figure 5, the bands around 1000 and 910  $\text{cm}^{-1}$ , attributed to the asymmetric stretching vibration of Si-O-Ge and symmetric vibration Ge-O-Ge in the framework,<sup>[24]</sup> disappeared for ECNU-21 (Si/Ge = 33 or 0.48  $\text{mmol g}^{-1}$  Ge content), due to the extensive removal of Ge atoms by 84.3% from the parent CIT-13 (Si/Ge = 3.7 or 3.06  $\text{mmol g}^{-1}$  Ge content). Meanwhile, the extraction of Ge species also made the band around 550  $\text{cm}^{-1}$  of CIT-13, attributed to the asymmetric Ge-O-Ge vibration,<sup>[24]</sup> blue shift to 580  $\text{cm}^{-1}$  for Ge-poor ECNU-21. The blue shift of 30  $\text{cm}^{-1}$  was caused by the major loss of heavier Ge atoms to result in a high-silica ECNU-21 zeolite, similar to that seen for high-silica zeolite CIT-13S (0.52  $\text{mmol g}^{-1}$  Ge content). Moreover, the pristine 580  $\text{cm}^{-1}$  band of CIT-13, related to the vibration of D4R units,<sup>[23]</sup> was absent for ECNU-21, indicating the deconstruction and removal of D4R units.

### Structure analysis of ECNU-21 zeolite

As has been revealed above, the Si-rich *cfi*-layers have been well-preserved in the hydrolysis and reassembly processes. Hence, the structural model of ECNU-21 zeolite was constructed by reconnecting adjacent ECNU-21P layers with oxygen linkage in a periodic manner, which resulted in the formation of a 3D zeolite with 1D 10-R channel system parallel to *c*-axis. The structure of the formed ECNU-21 zeolite was optimized fully (optimizing fractional coordinates and the unit-cell volume and shape) using Materials Studio. Figure 6 shows the simulated PXRD pattern



**Figure 6.** Rietveld refinement of the PXRD data for ECNU-21. Experimental (black) and calculated (red) PXRD patterns, as well as the difference profile, are shown (blue). The short tick marks (green) below the patterns give the positions of the Bragg reflections.

matched well with the experimental data, indicating the daughter structure ECNU-21 was highly crystalline. According to the refined structure, ECNU-21 possessed the unit-cell parameters of  $a = 17.1516$  Å,  $b = 13.7371$  Å and  $c = 5.0289$  Å with the space group *Cmmm* (65) (Table S3-S7). The refinement of the unit-cell exhibited that the lattice parameters *a* decreased from ~27.4 Å for reported CIT-13 ( $a = 27.4374$  Å,  $b = 13.8000$  Å,  $c = 10.2910$  Å) to

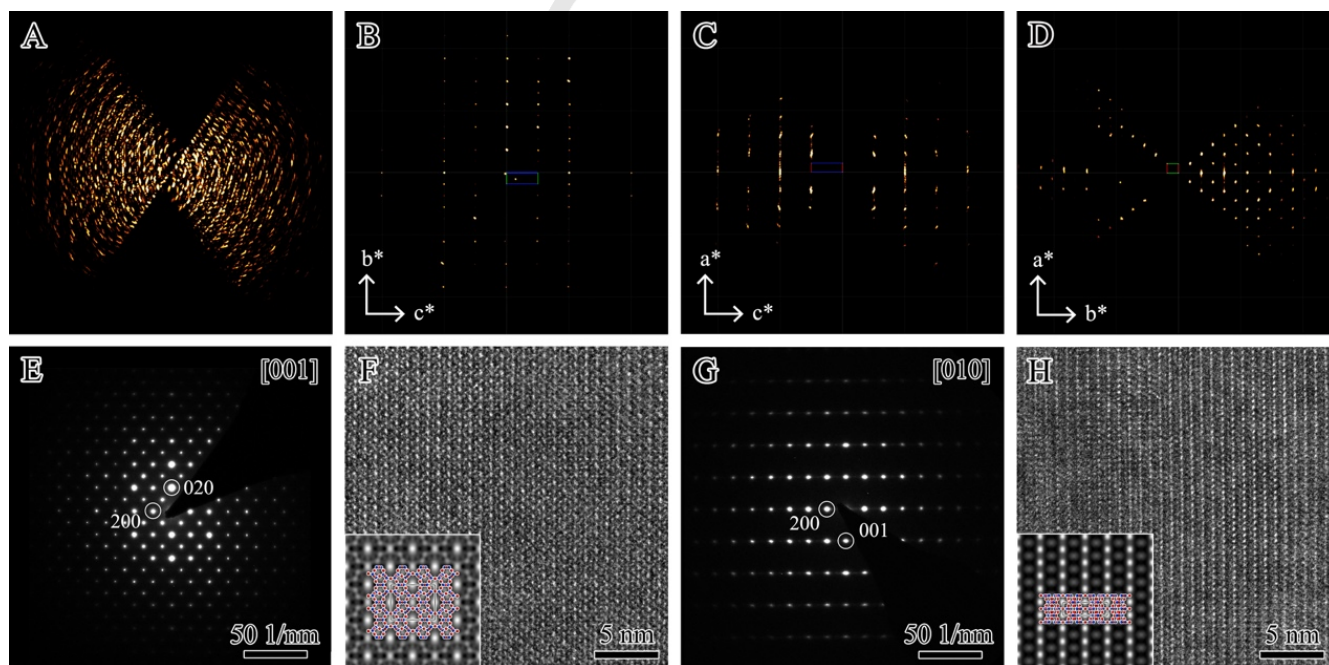
## FULL PAPER

~17.2 Å for ECNU-21. Thus, the difference of interlayer distance between CIT-13 and ECNU-21 was ca. 5.1 Å (half of a value represents the interlayer spacing, Scheme 1), in good agreement with the length of D4R linkage removed in the alkaline media. The *b* value was almost identical with that of CIT-13, meaning the silica-rich layers were well-preserved in the structural transformation process. As the random distribution of D4R subunits along *c*-axis was selectively removed by alkaline treatment, the lattice parameters *c* was reduced by half.

To verify the presence of highly ordered structure in ECNU-21, the investigation has been carried out using 3D electron diffraction tomography (3D-EDT).<sup>[25]</sup> The 3D-EDT data set was collected in the range of -60.4° to +52.2° with a beam-tilt step of 0.1°. From the acquired data set, 3D reciprocal space was reconstructed using the software EDT Process (Figure 7A). The unit-cell parameters calculated from 3D-EDT were *a* = 17.00 Å, *b* = 13.57 Å and *c* = 4.96 Å, which are consistent with the results from PXRD data. The observed reflection conditions were summarized as *hkl*: *h* + *k* = 2*n*; *0kl*: *k* = 2*n*; *h0l*: *h* = 2*n*; *hk0*: *h* + *k* = 2*n*; *h00*: *h* = 2*n*; *0k0*: *k* = 2*n*, which suggests four possible space groups—*C222* (21), *Cmm2* (35), *Cm2m* (38) and *Cmmm* (65). According to the plane groups of the high-resolution transmission electron microscopy (HRTEM) images (*vide post*), *C222* and *Cmmm* are both consistent. However, considering the original structure, synthesis process, and PXRD data, the space group *Cmmm* (65) is chosen. The cuts of reconstructed reciprocal lattice from three main directions contain sharp diffraction spots, showing high crystal-structural coherence (Figure 7B-D). The selected-area electron diffraction (SAED) pattern taken along [001] direction

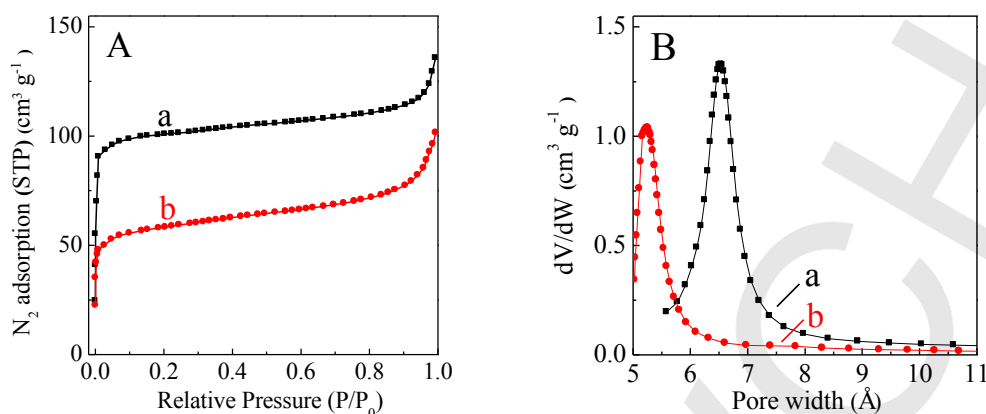
shown in Figure 7E is consistent with the 3D-EDT results. The corresponding HRTEM image has been taken for further confirmation of the structure, which allows the observation of well-ordered 10-R channels in the sample (Figure 7F). The averaged structural feature was obtained from Fourier transform of the raw HRTEM image using the crystallographic image processing software CRISP,<sup>[26]</sup> for which *c2mm* symmetry is chosen. In an attempt to gain some insight to the degree of ordering in ECNU-21, we further acquired the SAED pattern (Figure 7G) and HRTEM (Figure 7H) from [010] direction. Both show a highly ordered framework structure with single crystal feature. The averaged structure was also obtained by the crystallographic image processing with *p2mm* symmetry applied. The structural model of ECNU-21 matches well with the averaged HRTEM image. Therefore, it further confirmed that the D4R units has been completely removed from the structure. There is no disorder in the projection along *b*-axis. Thus, it can be concluded that ECNU-21 comprises only O-linkages between exactly the same layers as the parent CIT-13 zeolite.

N<sub>2</sub> adsorption in Figure 8A manifested that the ECNU-21 zeolite was a typical microporous material with lower specific surface area and micropore volume than the pristine CIT-13 zeolite (376 m<sup>2</sup> g<sup>-1</sup> and 0.06 cm<sup>3</sup> g<sup>-1</sup> vs. 579 m<sup>2</sup> g<sup>-1</sup> and 0.17 cm<sup>3</sup> g<sup>-1</sup>; Table S8), caused by the pore shrinkage and framework density increase upon the removal of D4R units. Intergrowth CIT-13, composed of intersected 14- and 10-R channels, exhibited one board pore size distribution around 6.5 Å according to Horvath-Kawazoe model (Figure 8B). After extensive removal of the D4R units and interlayer condensation process, the resultant ECNU-21 zeolite



**Figure 7.** (A) Projection of three-dimensional reciprocal space reconstructed from the 3D-EDT data. Three cuts of reconstructed reciprocal lattice giving two-dimensional slices of *0kl* (B), *h0l* (C) and *hk0* (D), respectively. (E) The SAED pattern of the crystal taken from [001] direction. (F) The corresponding HRTEM image. (G) The SAED pattern of the crystal taken from [010] direction. (H) The corresponding HRTEM image. Inserts are the corresponding averaged TEM images obtained by crystallographic image processing with *c2mm* and *p2mm* symmetry applied, respectively. The structural models are both superimposed.

## FULL PAPER



**Figure 8.** N<sub>2</sub> adsorption isotherms (A) at 77 K and pores size distribution (Horvath-Kawazoe method) (B) based on Ar adsorption at 87 K of calcined CIT-13 (a) and ECNU-21 (b).

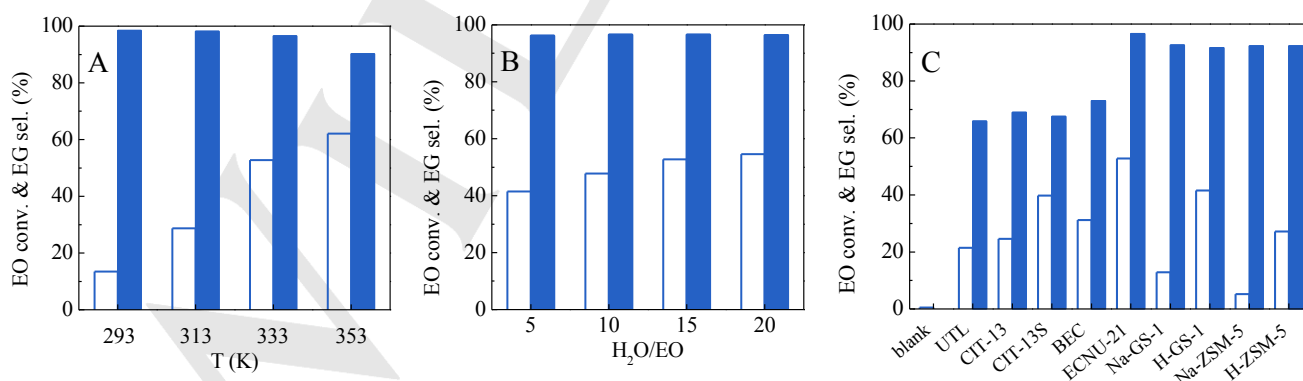
possessed a smaller pore size centered at 5.2 Å corresponding to the 10-R channels running along *c*-axis.

#### Catalytic performance of ECNU-21 in epoxide hydration

The newly formed pure crystalline ECNU-21 zeolite was characteristic of high-silica nature and hydrothermal stability compared to the pristine Ge-rich CIT-13 zeolite. Nevertheless, ECNU-21 still possessed a Ge content of 0.48 mmol g<sup>-1</sup>, corresponding to Si/Ge = 33. The framework Ge ions exhibited Lewis acidity as evidenced by pyridine-IR spectra (Figure S11). Taking the advantage of unique 10-R channels and Ge-related Lewis acidity, ECNU-21 was expected to serve as a promising shape-selective catalyst for processing important petrochemical reactions, *e.g.* the hydration of ethylene oxide (EO) to ethylene glycol (EG), a bulk chemical with a world market of 28 million tons per year by 2015.<sup>[27]</sup> Conventionally, the EO hydration was conducted in non-catalytic way in industrial process, but with an extremely high H<sub>2</sub>O/EO molar ratio of 20 - 25 at elevated

temperatures (423 - 493 K), which is highly energy-consuming in the separation of EG product. Using unstable acidic resins as the catalysts, the H<sub>2</sub>O/EO ratio was possibly decreased to 8, while keep a EG selectivity high as 95.6% at 378 K.<sup>[28]</sup> Recently, a heterogeneous catalyst Sn-SSZ-13 with active Sn sites confined in Chabazite cages has made a key breakthrough for EO hydration at approaching stoichiometric H<sub>2</sub>O/EO ratio.<sup>[29]</sup> As Sn and Ge are the congeners, they are presumed to have similar chemical and catalytic characteristics.

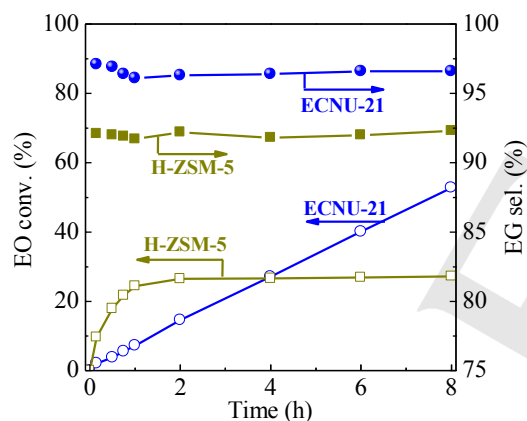
The reaction parameters of the EO hydration over ECNU-21 zeolite were firstly examined in detail. A significant temperature effect on the catalytic performance of ECNU-21 zeolite was observed when the reaction was carried out in the temperature range of 293 - 353 K (Figure 9A). Increasing the reaction temperature promoted the EO conversion from 13.5% to 62.1%, but resulted in a distinct decline of the EG selectivity by > 8%, because higher reaction temperatures may induce the further condensation of EG to diethylene glycol (DEG) at the outer surface of ECNU-21 zeolite.<sup>[29]</sup> Elevating H<sub>2</sub>O/EO ratio played a weak positive role on the EO conversion but did not affect EG



**Figure 9.** (A) Effect of reaction temperature on the EO conversion (blank) and EG selectivity (solid) for the EO hydration catalyzed by ECNU-21 catalyst. Reaction conditions: cat., 0.3 g; EO, 10 mmol; H<sub>2</sub>O, 150 mmol; time, 8 h. (B) Effect of H<sub>2</sub>O/EO ratio on the EO conversion (blank) and EG selectivity (solid) for the EO hydration catalyzed by ECNU-21 catalyst. Reaction conditions: cat., 0.3 g; EO, 10 mmol; temp., 333 K; time, 8 h. (C) EO conversion (blank) and EG selectivity (solid) in the EO hydration catalyzed by different zeolite catalysts. Reaction conditions: cat., 0.3 g; EO, 10 mmol; H<sub>2</sub>O, 150 mmol; temp., 333 K; time, 8 h.

## FULL PAPER

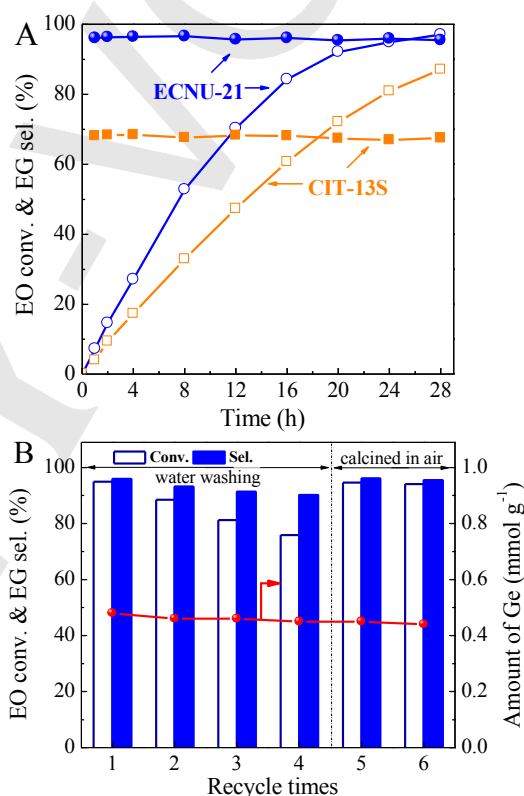
selectivity keeping at ca. 96% (Figure 9B). Hence, ECNU-21 was capable to catalyze EO hydration reaction, providing a high EO conversion (52.8%) and EG selectivity (96.6%) at 333 K with H<sub>2</sub>O/EO ratio of 15, that is, under extremely mild conditions in comparison to conventional non-catalytic process. Under the identical conditions, the catalytic performance of as-designed zeolite ECNU-21 in the EO hydration was compared to other germanosilicates and aluminosilicates (Figure 9C and Table S9). No products could be detected without any catalyst, while considerable EO conversions (5.2% - 52.8%) were obtained with the catalysts investigated in present study. Moreover, the ECNU-21 zeolite exhibited the highest EG selectivity of 96.6% at 8 h, followed by H-ZSM-5 (~92.3%) and H-GS-1 (~91.7%) catalysts. In contrast, the selectivity obtained by large and extra-large pores germanosilicates (UTL, CIT-13, CIT-13S, BEC) were only ~70%. The by-product was DEG with larger molecular dimension than EG, suggesting that the open pore system favored the further condensation of EG and EO. Furthermore, the sodium-type zeolites, Na-GS-1 and Na-ZSM-5, exhibited an apparent decrease in catalytic activity than H-GS-1 and H-ZSM-5 as a result of losing a large amount of the acid sites. The framework structure was well-preserved after the reaction for ECNU-21, CIT-13S and MFI-type zeolites (Figure S12).



**Figure 10.** Dependence of EO conversion (blank) and EG selectivity (solid) on reaction time in the EO hydration over ECNU-21 and H-ZSM-5. Reaction conditions: cat., 0.3 g; EO, 10 mmol; H<sub>2</sub>O, 150 mmol; temp., 333 K.

Despite of the comparable 10-R pore channels, germanosilicate ECNU-21 with weaker acidity showed a higher ability for converting EO to EG in comparison to aluminosilicate H-ZSM-5 with stronger acidity (Figure 9C). In order to clarify this phenomenon, we have compared the time course of EO hydration over ECNU-21 and H-ZSM-5 (Figure 10). H-ZSM-5 exhibited a higher initial EG conversion than ECNU-21 during the first 2 h possibly due to its stronger acidity. And the conversion was maintained at ~27% irrespective of prolonging the time, indicating the extremely fast deactivation of H-ZSM-5 after 2 h. In contrast, the EO conversion over ECNU-21 displayed a linear relationship with reaction time, reaching 52.8% at 8 h. In order to illustrate the significantly different resistance to the deactivation in the hydration of EO between ECNU-21 and H-ZSM-5, the removal of EG adsorbed in ECNU-21 and H-ZSM-5 were compared by TG

analysis and *in-situ* IR. EG/ECNU-21 and EG/H-ZSM-5 both showed weight loss in the temperature range of 298 - 1073 K (Figure S13). In the case of EG/ECNU-21, the first stage (298 - 400 K) corresponded to the removal of the physically adsorbed water, and the second one, in the temperature range of 400 - 450 K, was assigned to the combustion of the physically adsorbed EG. With respect to EG/H-ZSM-5, it displayed wider temperature range (400 - 600 K) including a small shoulder peak around 520 K in the second stage, indicating that the removal of adsorbed EG from H-ZSM-5 was more difficult in comparison to ECNU-21. A similar phenomenon has also been observed in the EG adsorption of Ti-MWW and H-MCM-22.<sup>[30]</sup> As shown in Figure S14, two bands emerged at 2885 and 2951 cm<sup>-1</sup> in the *in-situ* IR spectra






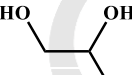
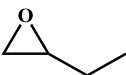
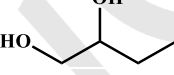
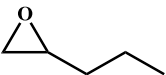
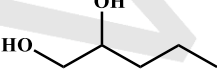
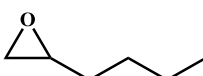
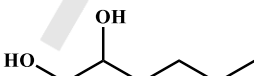
**Figure 11.** (A) Dependence of EO conversion (blank) and EG selectivity (solid) on reaction time in the EO hydration over ECNU-21 and CIT-13S catalysts. Reaction conditions: cat., 0.3 g; EO, 10 mmol; H<sub>2</sub>O, 150 mmol; temp., 333 K. (B) EO conversion (blank), EG selectivity (solid) and the change of Ge content in the recycling test for EO hydration over ECNU-21 catalyst. Reaction conditions: cat., 0.3 g; EO, 10 mmol; H<sub>2</sub>O, 150 mmol; temp., 333 K; reaction time for reuse, 24 h. The used ECNU-21 catalyst was regenerated by washing with deionized water or further calcination in air at 823 K for 6 h

that are assigned to symmetrical and asymmetrical stretching CH<sub>2</sub> groups, respectively.<sup>[31]</sup> These bands should be closely related to EG and decreased in intensity with raising the desorption temperature for EG/ECNU-21. On the contrary, these bands are more resistant against evacuation for EG/H-ZSM-5, indicative of a stronger interaction between EG and H-ZSM-5. Hence, it was reasonable that H-ZSM-5 suffered a faster deactivation than ECNU-21, because the product of EG could not desorb easily from H-ZSM-5 and then possibly caused a carbon deposition on



## FULL PAPER

**Table 1.** Hydration of various epoxides over ECNU-21 catalyst<sup>[a]</sup>.

No.	Substrate	Conv. / %	Product	Sel. / %
1		52.8		96.6
2		35.7		96.1
3		34.1		96.7
4		30.2		96.9
5		28.4		97.4

[a] Reaction conditions: cat., 0.3 g; substrate, 10 mmol; H<sub>2</sub>O, 150 mmol; temp., 333 K; time, 8 h.

the Al active sites.

Especially, ECNU-21 also showed a gradually increased activity with prolonging reaction time and reached a remarkable catalytic performance of 97.1% EO conversion at 28 h together with a steady EG selectivity of 95.5% (Figure 11A). The main by-product was DEG with a selectivity merely 4.5%. On the contrary, the framework-stabilized CIT-13S, with the same building layers as that of ECNU-21 but larger 14×10-R channels, gave a lower EO conversion of 87.1% and much lower EG selectivity of 67.5%. The extra-large pores are non-shape selective and could not suppress the dimerization of EG, with the DEG selectivity up to 32.5%. An obviously decrease in activity (e.g., EO conversion from 94.9% to 75.9%) was observed within four cycles when the used ECNU-21 catalyst was just washed with deionized water for reuse (Figure 11B). However, the catalytic activity could be fully recovered when the used catalyst was further calcined to remove any organic species. The deactivation of ECNU-21 is presumed to be caused mainly by coke formation. Besides, the Ge content was almost constant during six reaction-regeneration cycles.

Inspired by the great success of zeolite ECNU-21 in EO hydration reaction, we further expanded to other epoxide substrates (epoxypropane, 1,2-epoxybutane, 1,2-epoxypentane and 1,2-epoxyhexane) producing the corresponding 1,2-diols (Table 1). Along with the increase of the substrate size, ECNU-21 lost its hydration activity gradually because of steric restrictions. When using bulky 1,2-epoxyhexane as substrate, the conversion dropped to 28.4%. It is worth highlighting that in the hydration of various epoxide substrates, the expected high 1,2-diol selectivity (> 96%) could be maintained by ECNU-21 catalyst due to a 10-R channel system. These results confirmed the feasibility of shape-

selective Lewis acid catalysis confined in the 10-R pores of ECNU-21 zeolite.

## Conclusions

In conclusion, an intergrowth Ge-CIT-13 with a large amount of Si-O-Si interlayer bonds (> 21%) in D4R units encountered failure to form a lamellar product under acidic circumstance. For the first time, a facial alkali treatment strategy was proposed to efficiently cleave the metastable Si-O-Si interlayer bonds vertical to layers, realizing the purification of polymorph CIT-13 into single crystalline ECNU-21 zeolite with a novel topology. With moderate Lewis acidity confined in ordered 10-R channels, ECNU-21 served as a promising selective catalyst in the EO hydration reaction with the EO conversion of > 97% and EG selectivity ca. 96%. The profound work deepens the knowledge in hydrolyzing Ge-containing zeolites and provides brand new ideas for extending the practical applications of germanosilicates.

## Experimental Section

Details for synthesizing the parent germanosilicate CIT-13, partial characterization, catalytic reaction and additional discussion are described in the Supplementary Information.

**Synthesis of high-silica zeolite ECNU-21.** The powder of calcined Ge-CIT-13 (Si/Ge molar ratio of 3.7) was immersed in 1.0 wt% NH<sub>3</sub>·H<sub>2</sub>O aqueous solution with a solid-to-liquid weight ratio of 1 : 100 at 298 K for 24 h in a Teflon-lined autoclave. This treatment induced pronounced

## FULL PAPER

structural changes to the CIT-13 framework. The solid was recovered by filtration, extensively washing with deionized water and drying overnight at 353 K, forming a layered precursor, denoted as ECNU-21P. The product was further calcined at 823 K for 6 h in air, inducing full interlayer condensation and then giving rise to stable ECNU-21 zeolite with 3D crystalline structure and novel high-silica framework (Si/Ge = 33).

**Structural modification of CIT-13 zeolite by acid treatment.** Following the traditional acid-assisted ADOR procedures, the structural change through hydrolysis of D4R units in CIT-13 framework was also attempted for control experiment. The acid treatment of the calcined CIT-13 sample was performed in HCl aqueous solution with changeable concentrations (0.1 - 4.0 M) at a solid-to-liquid weight ratio of 1 : 100 and at 368 K for 16 h. After being filtrated, washed and dried, the obtained solids were calcined at 823 K for 6 h.

To further investigate the structural change of CIT-13, hydrolysis treatment was carried out by following our previously reported procedures.<sup>[19]</sup> The CIT-13 zeolite in calcined form was soaked in 1 M HNO<sub>3</sub> aqueous solution with a solid-to-liquid weight ratio of 1 : 100, and the mixture was heated in a Teflon-lined autoclave at 443 K for a different period of times (15 min - 24 h). Hydrolysed samples were then recovered with the same abovementioned procedures. Note that the sample obtained by HNO<sub>3</sub> treatment for 2 h exhibited a PXRD pattern same as pristine CIT-13 zeolite, implying the HNO<sub>3</sub> treatment only stabilized the \*CTH framework but did not cause effective structural degradation as reported before.<sup>[19]</sup> The resultant material is denoted as CIT-13S (Si/Ge = 30).

#### Characterization methods

Powder X-ray diffraction (PXRD) patterns were collected on a Rigaku Ultima IV X-ray diffractometer using CuK $\alpha$  radiation ( $\lambda$  = 1.5406 Å, 35 kV, 25 mA). High resolution data for determining the ECNU-21 structure by Rietveld refinement were recorded on a Bruker D8 Advance X-ray diffractometer using CuK $\alpha$  radiation (35 kV, 25 mA) with an incident monochromatic X-ray wavelength of 1.5406 Å. To improve accuracy, the sample was continuously rotated in a 0.5 mm glass capillary. The *in-situ* PXRD measurements were also carried out on Bruker D8 Advance X-ray diffractometer with a wavelength 1.5406 Å. The ECNU-21P sample was packed in air at ambient pressure inside ceramic plate and heated from 298 to 873 K with a ramp rate of 30 K min<sup>-1</sup>. The high-resolution transmission electron microscopy (HRTEM) images were collected with a FEI G2F30 with an accelerating voltage of 300 kV. The 3D-EDT data collected on a JEOL JEM-2100 microscope that was equipped with a LaB6 gun operated at 200 kV (Cs 1.0 mm, point resolution of 2.3 Å). A TENGRA CCD camera (2304 × 2304 pixels with a 2:1 fiber-optical taper and an effective pixel size of 18  $\mu$ m<sup>2</sup>) was used for digital recording of the diffraction pattern. The collected dataset was processed using the EDT Process software. N<sub>2</sub> adsorption isotherms were recorded at 77 K on a BELSORP-MAX instrument after activating the calcined samples at 573 K for at least 10 h under vacuum conditions. The pore size distribution was calculated by the Horvath-Kawazoe (HK) method based on the data collected by Ar adsorption at 87 K on a Micromeritics ASAP2020 adsorption instrument. The IR spectra in the zeolite framework vibration region were collected on a Nicolet Nexus 670 FT-IR spectrometer in absorbance mode using KBr technique (6 wt% wafer). The Si, Ge, Al and Na contents were measured with inductively coupled plasma (ICP) spectroscopy on a Thermo IRIS Intrepid II XSP atomic emission spectrometer. Solid-state <sup>29</sup>Si MAS NMR spectra were measured on a VARIAN VNMR5 400WB NMR spectrometer using single-pulse method at a frequency of 79.43 MHz, a spinning rate of 3 kHz, and a recycling delay of 60 s. The chemical shift was referred to [(CH<sub>3</sub>)<sub>3</sub>SiO]<sub>4</sub>SiO<sub>12</sub>. The <sup>19</sup>F MAS NMR spectrum of pristine CIT-13 was acquired at 9.4 T on a Varian Infinity

Plus 400 WB spectrometer using a 2.5 mm HX MAS probe. The chemical shift was referenced to trifluoroacetic acid at -76.55 ppm.

#### Structure analysis

The powder diffraction patterns of ECNU-21 was indexed with the program X-Cell<sup>[32]</sup> and the software of Materials Studio<sup>[33]</sup>. The crystalline structure was refined with FULLPROF.<sup>[34]</sup> Structure refinement of the diffraction data of ECNU-21 was started in *Cmmm* (65) space group. All the atoms were refined isotropically, while neutral scattering factors were employed for them. The background curve was fitted by using the linear interpolation between a set background points with refinable heights. Soft restraints were placed on the bond distances of the framework throughout the refinement. On the basis of the HRTEM images of ECNU-21, a structure model was derived and subjected to geometry optimization using the quantum mechanical code Dmol<sup>3</sup> in the Materials Studio suite of programs. The exchange-correlation functional was expressed by the generalized gradient corrected (GGA) functional by Perdew-Burke-Ernzerh parametrization. Crystallographic image processing on HRTEM images was carried out using the program CRISP.<sup>[26]</sup> The simulations of the TEM images were performed using the MacTempas software.

#### Catalytic reactions

The catalytic hydration of various epoxides (ethylene oxide, epoxypropane, 1,2-epoxybutane, 1,2-epoxypentane and 1,2-epoxyhexane) were performed under vigorous stirring in an autoclave reactor equipped with a Teflon-inner. In a typical experiment, a mixture of catalyst (0.3 g), epoxides (10 mmol) and H<sub>2</sub>O (150 mmol) was vigorously stirred at 333 K. The effect of both reaction temperature (293 - 353 K) and H<sub>2</sub>O/EO molar ratio (5 - 20) on the catalytic performance of ethylene oxide (EO) hydration on ECNU-21 were also investigated.

The recycling tests were performed to investigate the recyclability of ECNU-21 catalyst. After each reaction, the used ECNU-21 catalyst was centrifuged, washed with deionized water and dried at 353 K overnight for reuse in the next cycle. To restore the initial activity level, the used catalyst was also regenerated with further calcination in air at 823 K for 6 h.

The products were separated from the reaction mixture by centrifugation and determined by a gas chromatograph (Shimadzu 2014) equipped with an Rtx®-Wax capillary column (30 m × 0.25 mm × 0.25  $\mu$ m) and FID detector using isopropanol (or cyclohexanone) as internal standard. The products formed were identified by a GC-MS (Agilent 6890 series GC system, 5937 network mass selective detector). The results of the hydration of EO were calculated as follows.

$$\text{EO conversion} = \frac{\text{moles of EG produced}}{\text{moles of EO in the feed}} \times 100\%$$

$$\text{EG selectivity} = \frac{\text{moles of EG product}}{\text{moles of products produced}} \times 100\%$$

#### Acknowledgements

The authors gratefully acknowledge the financial support from NSFC of China (21533002, 21603075 and 21571128), China Ministry of Science and Technology (2016YFA0202804), National Excellent Doctoral Dissertation of China (201454), Shanghai Rising-Star Program (17QA1401700).

## FULL PAPER

## Conflict and interest

The authors declare no conflict of interest.

**Keywords:** topotactic conversion • intergrowth • ordered • germanosilicate • hydration reaction

- [1] A. Corma, *Chem. Rev.* **1997**, 97, 2373-2420.
- [2] Ch. Baerlocher, L. B. McCusker, Database of Zeolite Structures. <http://www.iza-structure.org/databases/>
- [3] a) R. L. Wadlinger, G. T. Kerr, E. J. Rosinski, *U.S. Patent* 3 308 069 **1967**; b) J. M. Newsam, M. M. J. Treacy, W. T. Koetsier, C. B. Gruyter, *Proc. R. Soc. London, Ser. A* **1988**, 420, 375-405; c) J. B. Higgins, R. B. LaPierre, J. L. Schlenker, A. C. Rohman, J. D. Wood, G. T. Kerr, W. J. Rohrbaugh, *Zeolite* **1988**, 8, 446-452.
- [4] a) M. A. Cambor, P. A. Barret, M. J. Díaz-Cabañas, L. A. Villaescusa, M. Puche, T. Boix, E. Perez, H. Koller, *Micropor. Mesopor. Mater.* **2001**, 48, 11-22; b) A. W. Burton, S. Elomari, I. Chan, A. Pradhan, C. Kibby, *J. Phys. Chem. B* **2005**, 109, 20266-20275.
- [5] a) T. Willhammar, J. L. Sun, W. Wan, P. Oleynikov, D. L. Zhang, X. D. Zou, M. Moliner, J. Gonzalez, C. Martinez, F. Rey, A. Corma, *Nat. Chem.* **2012**, 4, 188-194; b) M. Moliner, J. Gonzalez, M. T. Portilla, T. Willhammar, F. Rey, F. J. Llopis, X. D. Zou, A. Corma, *J. Am. Chem. Soc.* **2011**, 133, 9497-9505.
- [6] a) L. Xu, X. Y. Ji, J. G. Jiang, L. Han, S. A. Che, P. Wu, *Chem. Mater.* **2015**, 27, 7852-7860; b) S. Smeets, Z. J. Berkson, D. Xie, S. I. Zones, W. Wan, X. D. Zou, M. F. Hsieh, B. F. Chmelka, L. B. McCusker, C. Baerlocher, *J. Am. Chem. Soc.* **2017**, 139, 16803-16812.
- [7] Z. B. Yu, Y. Han, L. Zhao, S. Huang, Q. Y. Zheng, S. Z. Lin, A. Córdova, X. D. Zou, J. L. Sun, *Chem. Mater.* **2012**, 24, 3701-3706.
- [8] T. Conradsson, M. S. Dadachov, X. D. Zou, *Micropor. Mesopor. Mater.* **2000**, 41, 183-191.
- [9] A. Corma, M. T. Navarro, F. Rey, J. Rius, S. Valencia, *Angew. Chem. Int. Ed.* **2001**, 40, 2277-2280.
- [10] R. F. Lobo, M. E. Davis, *J. Am. Chem. Soc.* **1995**, 117, 3766-3779.
- [11] R. Castañeda, A. Corma, V. Fornes, F. Rey, J. Rius, *J. Am. Chem. Soc.* **2003**, 125, 7820-7821.
- [12] a) B. W. Boal, M. W. Deem, D. Xie, J. H. Kang, M. E. Davis, S. I. Zones, *Chem. Mater.* **2016**, 28, 2158-2164; b) J. H. Kang, D. Xie, S. I. Zones, S. Smeets, L. B. McCusker, M. E. Davis, *Chem. Mater.* **2016**, 28, 6250-6259.
- [13] Z. H. Gao, F. J. Chen, L. Xu, L. Sun, Y. Xu, H. B. Du, *Chem. Eur. J.* **2016**, 22, 14367-14372.
- [14] D. S. Firth, S. A. Morris, P. S. Wheatley, S. E. Russell, A. M. Z. Slawin, D. M. Dawson, A. Mayoral, M. Opanasenko, M. Polozij, J. Čejka, P. Nachtigall, R. E. Morris, *Chem. Mater.* **2017**, 29, 5605-5611.
- [15] W. J. Roth, P. Nachtigall, R. E. Morris, P. S. Wheatley, V. R. Seymour, S. E. Ashbrook, P. Chlubná, L. Grajciar, M. Polozij, A. Zukal, O. Shvets, J. Čejka, *Nat. Chem.* **2013**, 5, 628-633.
- [16] P. Chlubná-Eliášová, Y. Y. Tian, A. B. Pinar, M. Kubu, J. Čejka, R. E. Morris, *Angew. Chem. Int. Ed.* **2014**, 53, 7048-7052.
- [17] M. Shamzhy, M. Opanasenko, Y. Y. Tian, K. Konyshova, O. Shvets, R. E. Morris, J. Čejka, *Chem. Mater.* **2014**, 26, 5789-5798.
- [18] V. Kasneryk, M. Shamzhy, M. Opanasenko, P. S. Wheatley, S. A. Morris, S. E. Russell, A. Mayoral, M. Trachta, J. Čejka, R. E. Morris, *Angew. Chem. Int. Ed.* **2017**, 56, 4324-4327.
- [19] X. Liu, L. Zhang, H. Xu, J. G. Jiang, M. M. Peng, P. Wu, *Appl. Catal. A*, **2018**, 550, 11-19.
- [20] N. Kasian, A. Tuel, E. Verheyen, C. E. A. Kirschhock, F. Taulelle, J. A. Martens, *Chem. Mater.* **2014**, 26, 5556-5565.
- [21] E. Verheyen, L. Joos, K. Van Havenbergh, E. Breynaert, N. Kasian, E. Gobechiya, K. Houthoofd, C. Martineau, M. Hinterstein, F. Taulelle, V. Van Speybroeck, M. Waroquier, S. Bals, G. Van Tendeloo, C. E. A. Kirschhock, J. A. Martens, *Nat. Mater.* **2012**, 11, 1059-1064.
- [22] N. Kasian, G. Vanbutsele, K. Houthoofd, T. I. Koranyi, J. A. Martens, C. E. Kirschhock, *Catal. Sci. Technol.* **2011**, 1, 246-254.
- [23] X. Liu, H. Xu, L. Zhang, L. Han, J. Jiang, P. Oleynikov, L. Chen, P. Wu, *ACS Catal.* **2016**, 6, 8420-8431.
- [24] C. S. Blackwell, *J. Phys. Chem.* **1979**, 83, 3251-3257.
- [25] a) M. Gemmi, P. Oleynikov, *Z. Kristallogr. - Cryst. Mater.* **2013**, 228, 51-58; b) E. Mugnaioli, I. Andrusenko, T. Schüler, N. Loges, R. E. Dinnebier, M. Panthöfer, W. Tremel, U. Kolb, *Angew. Chem. Int. Ed.* **2012**, 51, 7041-7045; c) Q. M. Sun, Y. H. Ma, N. Wang, X. Li, D. Y. Xi, J. Xu, F. Deng, K. B. Yoon, P. Oleynikov, O. Terasaki, J. H. Yu, *J. Mater. Chem. A* **2014**, 2, 17828-17839.
- [26] S. Hövöller, *Ultramicroscopy* **1992**, 41, 121-135.
- [27] J. F. Pang, M. Y. Zheng, R. Y. Sun, A. Q. Wang, X. D. Wang, T. Zhang, *Green Chem.* **2016**, 18, 342-359.
- [28] F. P. Yu, H. Cai, W. J. He, W. M. Yang, Z. K. Xie, *J. Appl. Polym. Sci.* **2010**, 115, 2946-2954.
- [29] W. L. Dai, C. M. Wang, B. Tang, G. J. Wu, N. J. Guan, Z. K. Xie, M. Hunger, L. D. Li, *ACS Catal.* **2016**, 6, 2955-2964.
- [30] X. Q. Lu, H. Xu, J. Y. Yan, W. J. Zhou, A. Liebens, P. Wu, *J. Catal.* **2018**, 358, 89-99.
- [31] G. Phaomei, E. S. Ningthoujam, W. R. Singh, N. S. Singh, M. N. Luwang, R. Tewari, R. K. Vatsa, *Opt. Mater.* **2010**, 32, 616-622.
- [32] M. A. Neumann, *J. Appl. Cryst.* **2003**, 36, 356-365.
- [33] *Materials Studio Release Notes v.6.1*; Accelrys Software: San Diego, CA, **2012**.
- [34] J. R. CARVAJAL, Short Reference Guide of the Program Fullprof, **2005**, [www.llb.cea.fr/fullweb/winplotr/winplotr.htm](http://www.llb.cea.fr/fullweb/winplotr/winplotr.htm)

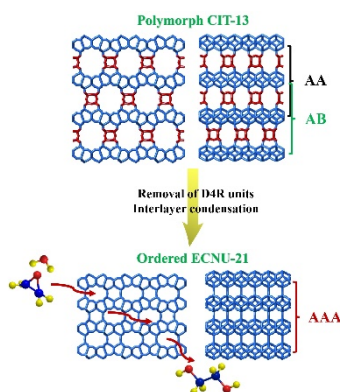
## FULL PAPER

## Entry for the Table of Contents (Please choose one layout)

Layout 1:

## FULL PAPER

Structural conversion from polymorph germanosilicate CIT-13 to novel ECNU-21 zeolite as shape-selective catalyst for ethylene oxide hydration



Xue Liu, Wenting Mao, Jingang Jiang, Xinqing Lu, Mingming Peng, Hao Xu,\* Lu Han,\* Shunai Che, Peng Wu\*

Page No. – Page No.

Topotactic conversion of alkali-treated intergrowth germanosilicate CIT-13 into single crystalline ECNU-21 zeolite as shape-selective catalyst for ethylene oxide hydration